Validation Report for "Automatic Satellite Image Interpretation" (ASII-PGE10 v2011)

NWC/CDOP3/GEO/ZAMG/SCI/VR/ASII, Issue 1.0

21 January 2019

Applicable to SAFNWC/MSG versions 2013, 2016 and 2018

The EUMETSAT Network of Satellite Application Facilities

NWC SAF
Support to Nowcasting and Very Short Range Forecasting

Prepared by ZAMG

REPORT SIGNATURE TABLE

Function	Name	Signature	Date
Prepared by	A. Wirth (ZAMG)		*21 January 2019*
Reviewed by	A. Jann (ZAMG) V. Meyer (ZAMG)		*21 January 2019*
Authorised by	Pilar Rípodas (AEMET) *SAFNWC Project Manager*		*21 January 2019*

DOCUMENT CHANGE RECORD

Version	Date	Pages	CHANGE(S)
1.0	21 January *2019*	24	Creation (actually, this is a re-release of SAF/NWC/CDOP2/ZAMG/SCI/VR/6 upon a corresponding request at the DRR for release of NWC/GEO v2018)

Table of contents

List of tables

List of figures

1. INTRODUCTION

1.1 SCOPE AND PURPOSE OF THE DOCUMENT

The Automatic Satellite Image Interpretation (ASII) algorithms implemented as PGE10 in v2011 of the SAFNWC / MSG software package have been developed in their initial version during the period 1997-2002 using the METEOSAT-7 imagery ([RD.2]), and been tuned afterwards using SEVIRI images ([RD.3]). The algorithms are detailed in the Algorithm and Theoretical Basis Document (ATBD) ([RD.1]).

This document is the continuation of the recently undertaken investigation on stability of the PGE10 product ([RD.4]). Main focus is laid on the stability of the pattern recognition modules used for the detection of the conceptual models. It was investigated how the output of the pattern recognition modules changes, when the pixel temperature values of the input (satellite image data) are slightly modified.

1.2 DEFINITIONS, ACRONYMS AND ABBREVIATIONS

ASII	Automatic Satellite Image Interpretation
BIGSLINE	Large S-shaped line
BT	Brightness Temperature
C_AREA	Contour Area
HEC	High Enhanced Cumulus
IR	Infra Red
LEC	Low Enhanced Cumulus
LONGFIB	Long Fibre cloud
MSG	Meteosat Second Generation
PGE	Product Generation Element
SEVIRI	Spinning Enhanced Visible and Infra-Red Imager
SLINE	S-shaped line
SMALLCC	Small Convective Cloud
WV	Water Vapour

1.3 REFERENCES

1.3.1 Applicable Documents

For dated references, subsequent amendments to, or revisions of, any of these publications do not apply. For undated references, the latest edition of the document referred to applies.

Latest documentation can be found at the SAFNWC Help Desk at http://nwc-saf.eumetsat.int

Ref	Title	Code	Vers	Date
[AD.1]	Project Plan for the NWCSAF CDOP3 phase	NWC/CDOP3/SAF/AEMET/MGT/PP	1.0	06/03/18
[AD.2]	NWCSAF CDOP3 Project Plan Master Schedule	NWC/CDOP3/SAF/AEMET/MGT/PP/MasterSchedule	1.1	28/02/18
[AD.3]	Configuration Management Plan for the NWC SAF	NWC/CDOP3/SAF/AEMET/MGT/CMP	1.0	21/02/18
[AD.4]	System and Components Requirements Document for the NWC/GEO	NWC/CDOP2/GEO/AEMET/SW/SCRD	2.1	21/01/19
[AD.5]	Interface Control Document for Internal and External Interfaces of the NWC/GEO	NWC/CDOP3/GEO/AEMET/SW/ICD/1	1.0	21/01/19
[AD.6]	Interface Control Document for the NWCLIB of the NWC/GEO	NWC/CDOP3/GEO/AEMET/SW/ICD/2	1.0	21/01/19
[AD.7]	Data Output Format	NWC/CDOP3/GEO/AEMET/SW/DOF	1.0	21/01/19
[AD.8]	Component Design Document for the NWCLIB of the NWC/GEO	NWC/CDOP2/GEO/AEMET/SW/ACDD/NWCLIB	2.0	27/02/17
[AD.9]	NWC SAF Product Requirements Document	NWC/CDOP3/GEO/AEMET/MGT/PRD	1.0	01/18
[AD.10]	User Manual for the Tools of the NWC/GEO	NWC/CDOP3/GEO/AEMET/SCI/UM/Tools	1.0	21/01/19

***Table 1**: List of Applicable Documents*

1.3.2 Reference Documents

The reference documents contain useful information related to the subject of the project. These reference documents complement the applicable documents. For dated references, subsequent amendments to, or revisions of, any of these publications do not apply. For undated references, the latest edition of the document referred to applies.

Latest documentation can be found at the SAFNWC Help Desk at http://nwc-saf.eumetsat.int.

Reference	Title	Code	Vers	Date
[RD.11]	Algorithm Theoretical Basis Document for the "Automatic Satellite Image Interpretation" product (ASII, PGE10)	SAF/NWC/CDOP/ZAMG/SCI/ATBD/10	2.3	02/02/11
[RD.12]	SAFNWC Scientific Report for MTR		1.0	02/2000
[RD.13]	Scientific report on First checking and Tuning for MSG PGE10	SAF/NWC/IOP/ZAMG/SCI/RP/2	1.0	07/01/04
[RD.4]	Validation Report for "Automatic Satellite Image Interpretation" product (ASII - PGE10 v2010)	SAF/NWC/CDOP/ZAMG/SCI/VR/4	1.0	20/04/10

Table 2: *List of Reference Documents*

2. GENERAL ASPECTS OF THE VALIDATION APPROACH

2.1 VALIDATION DATASET

A validation dataset containing 30 cases was used, comprising scenes from summer 2011 (25th July to 11th August 2011). The area under investigation is shown in Figure 1, capturing Europe and parts of the Atlantic. For each PGE10 run a grid with 127 x 91 grid points on the re-projected MSG image (Figure 2) was used. The mean distance between the grid points is approx. 70 km in east-west direction and approx. 50 km in north-south direction.

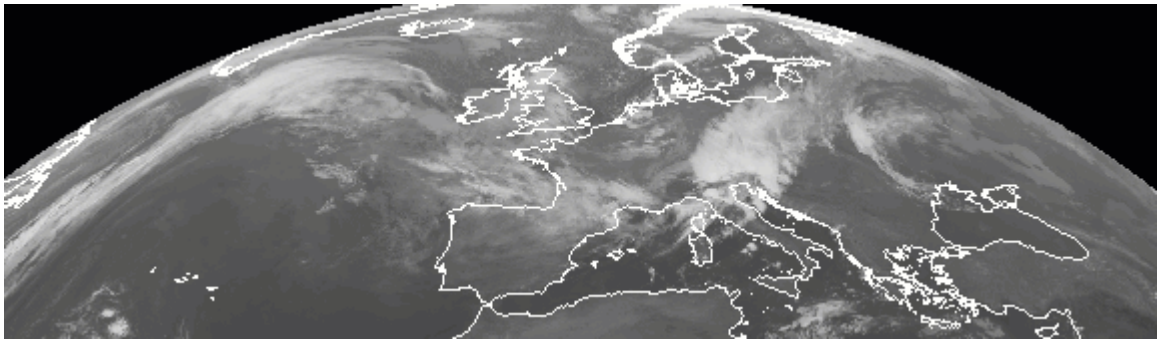

Figure 1: *Selected area from MSG image data comprising 2200 pixels in east-west and 650 pixels in north-south direction.*

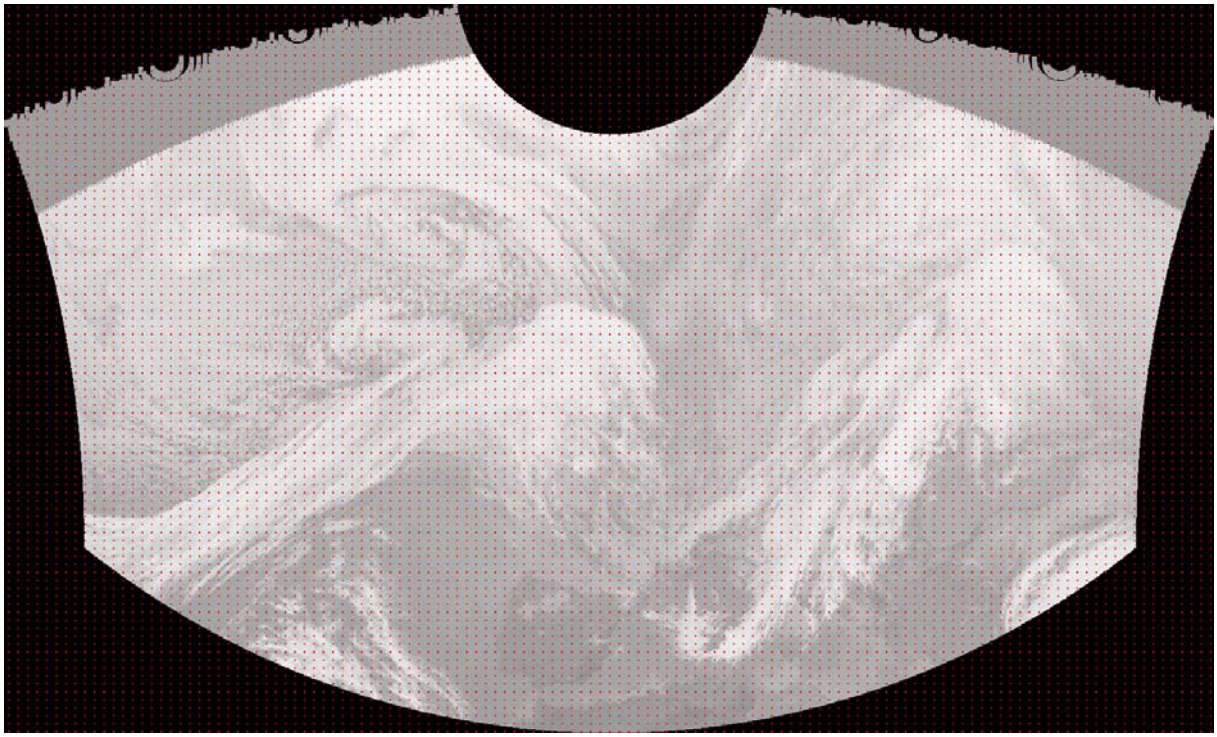

Figure 2: *Re-projected MSG image. A regular grid with 127 x 91 grid points was superimposed.*

2.2 METHODOLOGICAL ASPECTS

Pattern recognition methods are used in PGE10 for the detection of conceptual models. Input data for these pattern recognition modules are satellite image data (IR10.8µm or WV6.2µm) from MSG. The pattern recognition modules investigate the satellite data on pixel basis. These modules are based on temperature threshold techniques. Image pixels which fulfil the criteria defined for certain conceptual patterns (e.g. S-shaped lines, convective cells or fibre clouds) are then assigned to a regular grid (127x91 grid points), where each grid mesh covers an area of approximately 70 by 50 km on the re-projected MSG image data.

The aim of the following investigation is to see how stable or similar image patterns are detected when the input data slightly changes. The input data were varied in the way that SEVIRI brightness temperatures (SEVIRI_BT) were increased and decreased by 1 and 2 Kelvin compared to the original temperature of the IR and WV image. For a better understanding, we call hereafter [SEVIRI_BT] **the reference run** corresponding to the original brightness temperatures of the IR and WV images and [SEVIRI_MBT] **the 4 test runs** with the **M**odified SEVIRI **B**rightness **T**emperatures.

The artificial increase and decrease of image temperature in the test runs affect all pixels in the same way, i.e. the temperature difference to neighbouring pixel remains unaffected.

The following pattern recognition modules were analysed:

- C_AREA: detection of coherent cloud pattern exceeding a certain size, typical for frontal systems (ATBD [RD.1] chapter 3.1.8)
- CONVEX: detection of convex or concave pattern, used for the detection of wave pattern at the rear side of frontal cloud bands (ATBD [RD.1] chapter 3.1.11)
- SLINE: detection of S-shaped cloud borders at the rear side of frontal cloud bands (ATBD [RD.1] chapter 3.1.10)
- BIGSLINE: detection of large S-shaped cloud borders at the rear side of frontal cloud bands (ATBD [RD.1] chapter 3.1.10)
- STRIPE: detection of dark bands in the WV imagery (ATBD [RD.1] chapter 3.1.13)
- HEC: detection of high reaching convective cells (ATBD [RD.1] chapter 3.1.12)
- LEC: detection of lower convective cells (ATBD [RD.1] chapter 3.1.12)
- SMALL: detection of small convective cells (ATBD [RD.1] chapter 3.1.12)
- LONGFIB: detection of cloud fibres (ATBD [RD.1] chapter 3.1.14)

The first approach to asses the stability of the pattern recognition tools counts the number of image grid points which were assigned by one of the above listed pattern recognition methods for each test and reference run.

For the temperature modified input image [SEVIRI_MBT] and also for the original brightness temperatures [SEVIRI_BT], we will have to count the **T**otal number of **G**rid **P**oints (TGP) fulfilling a certain pattern [PAT] for all 11557 grid points of the grid and for all 30 cases of the validation data set:

GP(i) = 1 if a pattern [PAT] is recognized and assigned to a grid point (i=1 to 11557); otherwise GP(i)=0.

$$TGP_{PAT,SEVIRI\_BT} = \sum_{i=1}^{11557} GP(i)_{PAT,SEVIRI\_BT} \quad (1a)$$

$$TGP_{PAT,SEVIRI\_MBT} = \sum_{i=1}^{11557} GP(i)_{PAT,SEVIRI\_MBT} \quad (1b)$$

In the next step, the **A**verage number of TGP over the 30 cases from the validation dataset has been calculated for all runs:

$$AGP_{PAT,SEVIRI\_BT} = \frac{\sum_{j=1}^{30} TGP(j)_{PAT,SEVIRI\_BT}}{30} \quad (2a)$$

$$AGP_{PAT,SEVIRI\_MBT} = \frac{\sum_{j=1}^{30} TGP(j)_{PAT,SEVIRI\_MBT}}{30} \quad (2b)$$

Then, the deviation (*ADev*) of the averages of the test runs $AGP_{PAT,SEVIRI\_MBT}$ from the averages of the reference run $AGP_{PAT,SEVIRI\_BT}$ has been calculated according to:

$$ADev_{PAT,SEVIRI\_MBT}[\%] = \frac{|\, AGP_{PAT,SEVIRI\_MBT} - AGP_{PAT,SEVIRI\_BT} \,| * 100}{AGP_{PAT,SEVIRI\_BT}} \quad (3)$$

In a second approach, we count again the number of grid points fulfilling a certain pattern [PAT] for all 11557 grid points of the grid and for all 30 cases of the validation data set as we have done in (1b). But in contrast to (1b), only those grid points assigned with the same pattern in the test and the reference runs were counted (i.e. the same pattern must have the same location in the grid for reference and test runs, as illustrated in figure 3).

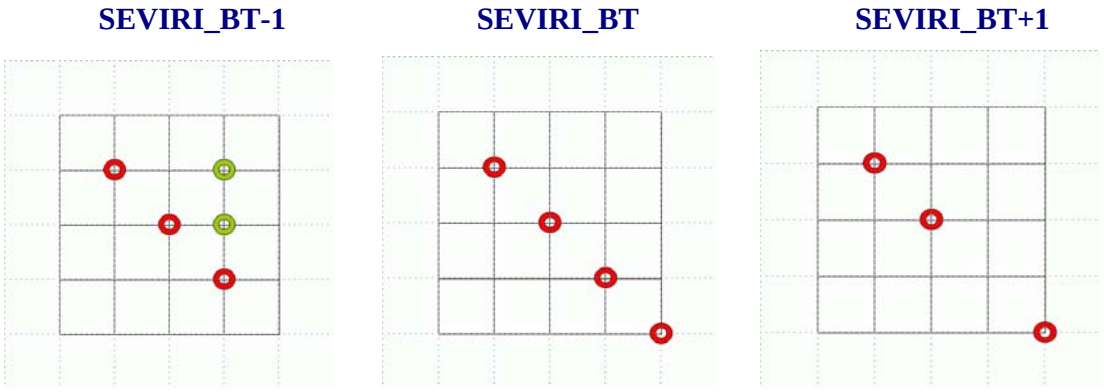

Figure 3: *Illustration of the diverging counting method. From left to right: Excerpts of the PGE10 grid with modified SEVIRI brightness temperature (-1 Kelvin) test run, reference run and test run with modified SEVIRI brightness temperature (+1 Kelvin) The identified patterns of interest are*

flagged by coloured grid points. Red grid points indicated that the same grid points are also flagged in the reference run, green grid points indicate that they have no counterparts in the reference run. While in the first attempt all grid points are counted, in the second attempt only the red flagged grid points are taken into account.

Again GP(i) = 1 if a pattern [PAT] is recognized and assigned to a grid point (i=1 to 11557); otherwise GP(i)=0.

$$TIGP_{PAT,SEVIRI\_MBT} = \sum_{i=1}^{11557} (GP(i)_{PAT,SEVIRI\_MBT} \equiv GP(i)_{PAT,SEVIRI\_BT} \equiv 1) \quad (4)$$

Where $TIGP_{PAT,\ SEVIRI\_MBT}$ is the **T**otal number of **I**dentically flagged **G**rid **P**oints between the test run [SEVIRI_MBT] and the reference run [SEVIRI_BT].

Similar to (2b), the **A**verage number of $TIGP_{PAT,SEVIRI\_MBT}$ from the test runs and $TIGP_{PAT,SEVIRI\_BT}$ from the reference runs over the 30 cases from the validation dataset has been calculated:

$$AIGP_{PAT,SEVIRI\_MBT} = \frac{\sum_{j=1}^{30} TIGP(j)_{PAT,SEVIRI\_MBT}}{30} \quad (5)$$

For the reference runs, equation (2a) is still valid:

$$AGP_{PAT,SEVIRI\_BT} = \frac{\sum_{j=1}^{30} TGP(j)_{PAT,SEVIRI\_BT}}{30} \quad (2a)$$

And finally, the deviation of the identically flagged grid points (*AIDev*) between the test runs $AIGP_{PAT,SEVIRI\_MBT}$ (equation 5) and the reference run $AGP_{PAT,\ SEVIRI\_BT}$ (equation 2a) has been calculated similar to equation (3):

$$AIDev_{PAT,SEVIRI\_MBT}[\%] = \frac{|\ AIGP_{PAT,SEVIRI\_MBT} - AGP_{PAT,SEVIRI\_BT}\ | * 100}{AGP_{PAT,SEVIRI\_BT}} \quad (6)$$

2.3 C_AREA: DETECTION OF COHERENT, EXTENDED CLOUD FEATURES

C_AREA	SEVIRI_BT-2	SEVIRI_BT-1	SEVIRI_BT	SEVIRI_BT+1	SEVIRI_BT+2
AGP	2415,16	2309,96	2116,7	2118,96	2024,33
ADev [%]	8,95	4,2	0	4,4	8,67

AIGP	2202,06	2197,36	2216,7	2101,13	2010,2
AIDev [%]	0,66	0,87	0	5,21	9,31

Table 3: *Results for the pattern recognition module C_AREA of the reference run SEVIRI_BT and 4 test runs with modified SEVIRI brightness temperatures.*

2.4 CONVEX: DETECTION OF CONVEX OR CONCAVE CLOUD PATTERN

CONVEX	SEVIRI_BT-2	SEVIRI_BT-1	SEVIRI_BT	SEVIRI_BT+1	SEVIRI_BT+2
AGP	114,3	103,13	98,4	91,73	93,5
ADev [%]	16,15	4,8	0	6,77	4,97
AIGP	67,1	76,83	98,4	72,2	64,93
AIDev [%]	31,8	21,92	0	26,62	34,01

Table 4: *Results for the pattern recognition module CONVEX of the reference run SEVIRI_BT and 4 test runs with modified SEVIRI brightness temperatures.*

2.5 SLINE: DETECTION OF S-SHAPED CLOUD BORDERS

SLINE	SEVIRI_BT-2	SEVIRI_BT-1	SEVIRI_BT	SEVIRI_BT+1	SEVIRI_BT+2
AGP	216,86	207,86	203,03	183,9	180
ADev [%]	6,81	2,37	0	9,42	11,34
AIGP	119,93	142,7	203,03	131	104,76
AIDev [%]	40,92	29,71	0	35,47	48,4

Table 5: *Results for the pattern recognition module SLINE of the reference run SEVIRI_BT and 4 test runs with modified SEVIRI brightness temperatures.*

2.6 BIGSLINE: DETECTION OF LARGE S-SHAPED CLOUD BORDERS

BIGSLINE	SEVIRI_BT-2	SEVIRI_BT-1	SEVIRI_BT	SEVIRI_BT+1	SEVIRI_BT+2

AGP	17,13	16,06	14,6	13,1	12,56
ADev [%]	17,32	10	0	10,27	13,97
AIGP	8,76	10,5	14,6	9,76	7,5
AIDev [%]	40	28,08	0	33,15	48,63

Table 6: *Results for the pattern recognition module BIGSLINE of the reference run SEVIRI_BT and 4 test runs with modified SEVIRI brightness temperatures.*

2.7 STRIPE: DETECTION OF DARK BANDS IN THE WV IMAGERY

STRIPE	SEVIRI_BT-2	SEVIRI_BT-1	SEVIRI_BT	SEVIRI_BT+1	SEVIRI_BT+2
AGP	459,13	457,63	452,2	454,83	454
ADev [%]	1,53	1,2	0	0,58	0,39
AIGP	431,6	433,63	452,2	437,5	428,06
AIDev [%]	4,55	4,1	0	3,25	5,33

Table 7: *Results for the pattern recognition module STRIPE of the reference run SEVIRI_BT and 4 test runs with modified SEVIRI brightness temperatures.*

2.8 HEC: DETECTION OF HIGH REACHING CONVECTIVE CELLS

HEC	SEVIRI_BT-2	SEVIRI_BT-1	SEVIRI_BT	SEVIRI_BT+1	SEVIRI_BT+2
AGP	19,03	17,3	16,26	15,1	13,26
ADev [%]	17,03	6,39	0	7,13	18,45
AIGP	14,1	15,26	16,26	14,3	12
AIDev [%]	13,28	6,15	0	12,05	26,19

Table 8: *Results for the pattern recognition module HEC of the reference run SEVIRI_BT and 4 test runs with modified SEVIRI brightness temperatures.*

2.9 LEC: DETECTION OF LOWER CONVECTIVE CELLS

LEC	SEVIRI_BT-2	SEVIRI_BT-1	SEVIRI_BT	SEVIRI_BT+1	SEVIRI_BT+2
AGP	13	12,63	12,06	11,3	10,63
ADev [%]	7,79	4,72	0	6,3	11,85
AIGP	10,1	11,3	12,06	10,46	9,06
AIDev [%]	16,25	6,3	0	13,26	24,87

Table 9: *Results for the pattern recognition module LEC of the reference run SEVIRI_BT and 4 test runs with modified SEVIRI brightness temperatures.*

2.10 SMALLCC: DETECTION OF SMALL CONVECTIVE CELLS

SMALLCC	SEVIRI_BT-2	SEVIRI_BT-1	SEVIRI_BT	SEVIRI_BT+1	SEVIRI_BT+2
AGP	129,76	131,3	132,06	132,56	132,1
ADev [%]	1,74	0,57	0	0,37	0,03
AIGP	106,83	117,9	132,06	122,2	113,23
AIDev [%]	19,1	10,72	0	7,46	14,25

Table 10: *Results for the pattern recognition module SMALLCC of the reference run SEVIRI_BT and 4 test runs with modified SEVIRI brightness temperatures.*

2.11 LONGFIB: DETECTION OF CLOUD FIBRES

SMALLCC	SEVIRI_BT-2	SEVIRI_BT-1	SEVIRI_BT	SEVIRI_BT+1	SEVIRI_BT+2
AGP	167,86	163,46	157,4	150,46	144,46
ADev [%]	6,64	3,85	0	4,4	8,22
AIGP	154,13	154,96	157,4	150,83	141,7
AIDev [%]	2,07	1,55	0	4,17	9,97

Table 11: *Results for the pattern recognition module LONGFIB of the reference run SEVIRI_BT and 4 test runs with modified SEVIRI brightness temperatures.*

3. INTERPRETATION OF THE RESULTS

Generally spoken, there is not one of the pattern recognition modules under investigation which remained unaffected when changing the brightness temperature of the satellite input data. All of the chosen pattern recognition modules depend in one or the other way on the measured temperatures in the satellite data, mainly because of the used threshold techniques. Therefore, a certain variation of the modules output was to be expected right from the beginning. Small dependencies should be called "stable" and strong variations of the output with input temperature "unstable".

There are two pattern recognition modules which revealed stable throughout the test runs: STRIPE and SMALLCC. While the first is derived from the WV imagery, the latter is computed from the IR image. Both modules show variations smaller than 2% for SEVIRI_MBT changes from -2 K to +2 K, when all flagged grid points were counted. In the second approach, i.e. when only identically labelled grid points were counted, the stability of the STRIPE module remained within an acceptable range below 5% variation, while the average variation for the SMALLCC module reached almost 20% for the test run [SEVIRI_BT-2].

The pattern recognition modules C_AREA, SLINE, LEC and LONGFIB show variation in the number of detected grids up to 10% approximately. Among these modules, LONGFIB is more stable than C_AREA, followed by SLINE and LEC. All 4 modules have in common, that they show a decrease in the number of flagged grid points when SEVIRI brightness temperature is increased.

Least stable are the modules CONVEX, BIGSLINE and HEC. They have in common, that at least for one of the test runs with modified SEVIRI brightness temperatures a deviation from the reference run of more than 15% occurred.

When observing *AIGP* and *AIDev [%]*, i.e. the number of grid points identically labelled in the test and reference runs, the deviation of the test runs from the reference run, increases dramatically for most investigated pattern recognition modules. From this point of view, the pattern recognition modules C_AREA, STRIPE and LONGFIB are best performing with variability up to 10% in the range SEVIRI_BT +/- 2 Kelvin. C_AREA and LONGFIB show lesser variation for the test runs [SEVIRI_BT-1] and [SEVIRI_BT-2] than for [SEVIRI_BT+1] and [SEVIRI_BT+2]. This asymmetry can be explained by the fact that both pattern recognition modules increase the number of the labelled grid points in comparison to the reference run when SEVIRI_BT is decreased. The pattern recognition modules CONVEX and SLINE show the same tendency but to a lesser extent for [SEVIRI_BT-2].

All other pattern recognition modules show a strong decrease in the number of detected identical grid points between test and reference run.

4. FURTHER INVESTIGATIONS ON STABILITY

4.1 GENERAL ASPECTS

In this section, instead of simply increasing or decreasing the temperature of the input satellite data by a given value as in chapter 2, a filtering method is applied on the temperature of each image pixel. The satellite data sample came from the same time period (25th July to 11th August 2011) and comprised again 30 cases. The subsequent statistical analysis remained the same as in part one (see chapters 2.1 and 2.2).

4.2 APPLIED FILTERING METHOD

A 3x3 filter was used for image smoothing on pixel basis. The algorithm used to alter the temperature information in the satellite data (IR10.8 and WV6.2) for the 4 test runs is:

$$\Delta T0 = T0 - \left(\frac{T1+T2+T3+T4+T5+T6+T7+T8}{8} \right) \quad (7)$$

$$T0_{res} = T0 + \alpha \, \Delta T0 \quad (8)$$

T1	T2	T3
T4	T0	T5
T6	T7	T8

Figure 4: *3x3 pixel array of the satellite input data with brightness temperatures T0 to T9.*

T1 to *T8* are the brightness temperature of the pixels surrounding the central pixel *T0*, and $T0_{res}$ the resulting brightness temperature of the central pixel. The reference run was performed with the original brightness temperatures and 4 test runs with values α=0.05 [=5%], α=0.1 [=10%],

α=0.15 [=15%] and α=0.2 [=20%], respectively, were carried out. The pattern recognition modules under investigation were the same as listed in the previous chapter 2.2.

4.3 C_AREA: DETECTION OF COHERENT, EXTENDED CLOUD FEATURES

C_AREA	reference run	5%	10%	15%	20%
AGP	2215,86	2213,3	2217,63	2216,76	2215,8
ADev [%]	0	-0,12	0,08	0,04	0
ADev [abs]	0	-2,56	1,77	0,9	-0,06
AIGP	2215,86	2189,83	2181,6	2176,63	2173,7
AIDev [%]	0	-1,17	-1,55	-1,77	-1,9
AIDev [abs]	0	-26,03	-34,26	-39,23	-42,16

Table 12: *Results for the pattern recognition module C_AREA of the reference run and the 4 test runs with modified SEVIRI brightness temperatures according to formula (7) and (8).*

4.4 CONVEX: DETECTION OF CONVEX OR CONCAVE CLOUD PATTERN

CONVEX	reference run	5%	10%	15%	20%
AGP	99,86	98,23	99,66	98,16	96,33
ADev [%]	0	-1,63	-0.2	-1.7	-3,53
ADev [abs]	0	-1,63	-0,2	-1,7	-3,53
AIGP	99,86	96,3	95,76	93,76	91,43
AIDev [%]	0	-3,56	-4,11	-6,11	-8,44
AIDev [abs]	0	-3,56	-4,1	-6,1	-8,43

Table 13: *Results for the pattern recognition module CONVEX of the reference run and the 4 test runs with modified SEVIRI brightness temperatures according to formula (7) and (8).*

4.5 SLINE: DETECTION OF S-SHAPED CLOUD BORDERS

SLINE	reference run	5%	10%	15%	20%
AGP	194,33	185,2	185,8	187,86	190,9
ADev [%]	0	-4,7	-4,39	-3,33	-1,92
ADev [abs]	0	-9,13	-8,53	-6,47	-3,73

AIGP	194,33	180,83	173,8	173,1	172,1
AIDev [%]	0	-6,95	-10,56	-10,92	-11,44
AIDev [abs]	0	-13,5	-20,53	-21,23	-22,23

Table 14: *Results for the pattern recognition module SLINE of the reference run and the 4 test runs with modified SEVIRI brightness temperatures according to formula (7) and (8).*

4.6 BIGSLINE: DETECTION OF LARGE S-SHAPED CLOUD BORDERS

BIGSLINE	reference run	5%	10%	15%	20%
AGP	14,46	14,53	14,4	14,43	14,4
ADev [%]	0	0,48	-0,41	-0,21	-0,41
ADev [abs]	0	0,07	-0,06	-0,03	-0,06
AIGP	14,46	14,26	14	13,9	13,6
AIDev [%]	0	-1,38	-3,18	-3,87	-5,95
AIDev [abs]	0	-0,2	-0,46	-0,56	-0,86

Table 15: *Results for the pattern recognition module BIGSLINE of the reference run and the 4 test runs with modified SEVIRI brightness temperatures according to formula (7) and (8).*

4.7 STRIPE: DETECTION OF DARK BANDS IN THE WV IMAGERY

STRIPE	reference run	5%	10%	15%	20%
AGP	450	450,53	450,9	454,03	455,86
ADev [%]	0	0,18	0,2	0,9	1,03
ADev [abs]	0	0,53	0,9	4,03	5,86
AIGP	450	448	447,06	446,63	446
AIDev [%]	0	-0,44	-0,65	-0,75	-0,89
AIDev [abs]	0	-2	-2,94	-3,37	-4

Table 16: *Results for the pattern recognition module STRIPE of the reference run and the 4 test runs with modified SEVIRI brightness temperatures according to formula (7) and (8).*

4.8 HEC: DETECTION OF HIGH REACHING CONVECTIVE CELLS

HEC	reference run	5%	10%	15%	20%
AGP	16,1	16,26	16,76	17,33	17,7
ADev [%]	0	0,99	4,11	7,64	9,94
ADev [abs]	0	0,16	0,66	1,23	1,6
AIGP	16,1	15,26	15,03	14,73	14,73
AIDev [%]	0	-5,22	-6,65	-8,51	-8,51
AIDev [abs]	0	-0,84	-1,07	-1,37	-1,37

Table 17: *Results for the pattern recognition module HEC of the reference run and the 4 test runs with modified SEVIRI brightness temperatures according to formula (7) and (8).*

4.9 LEC: DETECTION OF LOWER CONVECTIVE CELLS

LEC	reference run	5%	10%	15%	20%
AGP	12,13	12,5	13,13	13,4	14
ADev [%]	0	3,05	8,24	10,47	15,42
ADev [abs]	0	0,37	1	1,27	1,87
AIGP	12,13	11,46	11,33	11,03	10,7
AIDev [%]	0	-5,52	-6,6	-9,07	-11,79
AIDev	0	-0,67	-0,8	-1,1	-1,43

Table 18: *Results for the pattern recognition module LEC of the reference run and the 4 test runs with modified SEVIRI brightness temperatures according to formula (7) and (8).*

4.10 SMALLCC: DETECTION OF SMALL CONVECTIVE CELLS

SMALLCC	reference run	5%	10%	15%	20%
AGP	131,46	134,86	137,03	139,83	143,26
ADev [%]	0	2,57	4,24	6,37	8,98
ADev [abs]	0	3,4	5,57	8,37	11,8
AIGP	131,46	125,96	123	121,06	119,23
AIDev [%]	0	-4,18	-6,44	-7,91	-9,3
AIDev [abs]	0	-5,5	-8,46	-10,4	-12,23

Table 19: *Results for the pattern recognition module SMALLCC of the reference run and the 4 test runs with modified SEVIRI brightness temperatures according to formula (7) and (8).*

4.11 LONGFIB: DETECTION OF CLOUD FIBRES

SMALLCC	reference run	5%	10%	15%	20%
AGP	158,93	162,7	164,36	169,6	174,3
ADev [%]	0	2,37	3,42	6,71	9,67
ADev [abs]	0	3,77	5,43	10,67	15,37
AIGP	158,93	156,26	153,86	152,86	152,43
AIDev [%]	0	-1,68	-3,19	-3,82	-4,09
AIDev [abs]	0	-2,67	-5,07	-6,07	-6,5

Table 20: *Results for the pattern recognition module LONGFIB of the reference run and the 4 test runs with modified SEVIRI brightness temperatures according to formula (7) and (8).*

5. INTERPRETATION OF THE RESULTS

Among the treated pattern recognition modules, 3 categories may be distinguished. These 3 categories are also reflected in the results of the investigations on stability.

5.1 MODULES BASED ON A SMOOTHED INPUT IMAGE (C_AREA, CONVEX, SLINE AND BIGSLINE)

Among the pattern recognition modules of the first category, the C_AREA module can be characterised as stable. This module operates on a Gauss-filtered IR image. The number of C_AREA flagged grid meshes is high and there is no noticeable deviation of the 4 test runs from the reference run. When the number of coinciding grid mashes are counted only, the deviation from the reference run is smaller than 2%.

The CONVEX and the SLINE modules are based on the contours of the C_AREA field. Both modules show deviations up to 5% in the test runs and are clearly biased towards smaller detection rates the more the IR image is smoothed. Deviations from the reference run are twice as high when CONVEX- or SLINE-flagged grid meshes coinciding with the reference run are counted only. Both modules cannot be called stable in respect to small variations of the input image.

The BIGSLINE algorithm reveals more stable than the CONVEX and SLINE modules. BIGSLINE grid meshes are infrequent, but once detected; image smoothing has no influence on the detection rate. Nevertheless it seems that the position of the BIGSLINE pattern slightly changes with the borders of the C_AREA field since the percentage of coinciding grid meshes of the test runs with the reference run decreases the more the image is smoothed.

5.2 MODULE BASED ON THE SMOOTHED WV IMAGE (STRIPE)

The only pattern recognition module in this category is the STRIPE module. This module detects black (dry), elongated areas in the WV imagery. This module can be rated as stable with a weak bias towards an increase of STRIPE flagged grid meshed the stronger the WV image is smoothed (positive deviation). If grid meshes identical with the reference run are counted only, the deviation lies below 1%.

5.3 MODULES DEALING WITH THE FULL IMAGE RESOLUTION (HEC, LEC, SMALL_CC AND LONGFIB)

The third category comprises pattern detection modules based on full image resolution. For each of the modules the algorithm searches after pixel brightness maxima typical for convective cells (HEC, LEC and SMALL_CC). These algorithms show high deviations, but the number of concerned grid meshes per test case is small. Even though the number of flagged grid meshes for each module increases the stronger the input image is smoothed, the number of identical grid meshes with the reference run decreases rapidly. None of these modules can be considered stable.

The fibre detection algorithm (LONGFIB) also looks for local brightness maxima, in this case for maxima aligned along a cloud fibre. Deviations of the test runs from the reference run reach almost 10% for the LONGFIB module and are clearly biased towards positive values. The LONGFIB module cannot be classified as stable.

5.4 CONCLUSIONS

Among the nine pattern recognition methods, only 2 of them revealed stable in the environment of PGE10: The detection of frontal areas (C_AREA) in IR imagery and the detection of black stripes (STRIPE) in WV imagery. Both modules have in common, that they start from strongly smoothed image data (Gauss pyramid image) and are therefore not prone to show strong variations when image data is additionally smoothed as done in the four test runs. Pattern detection algorithms based on pixel data, trying to identify small scale image features (e.g. HEC, LEC and SMALL_CC) are more susceptible to changes than algorithms based on already smoothed images, trying to detect large coherent areas (e.g. C_AREA and STRIPE).

The sub-group of pattern recognition methods based on the contour line of the C_AREA (e.g. SLINE, CONVEX and BIGSLINE) show higher deviations from the reference run than the pattern they are based on (i.e. C_AREA). Still they are better performing than the pattern detection modules based on the higher resolution pixel basis.